Review of Scientific Instruments

EWALD: A macromolecular diffractometer for the second target station

Cite as: Rev. Sci. Instrum. **93**, 064103 (2022); https://doi.org/10.1063/5.0090810
Submitted: 09 March 2022 • Accepted: 07 May 2022 • Published Online: 08 June 2022

Gloria E. O. Borgstahl, William B. O'Dell, Martin Egli, et al.

Review of Scientific Instruments ARTICLE scitation.org/journal/rsi

EWALD: A macromolecular diffractometer for the second target station

Cite as: Rev. Sci. Instrum. 93, 064103 (2022); doi: 10.1063/5.0090810
Submitted: 9 March 2022 • Accepted: 7 May 2022 •
Published Online: 8 June 2022

Gloria E. O. Borgstahl,[1] William B. O'Dell,[2] Martin Egli,[3] Jan F. Kern,[4] Andrey Kovalevsky,[5] Jiao Y. Y. Lin,[6] Dean Myles,[5] Mark A. Wilson,[7] Wen Zhang,[8] Petrus Zwart,[9] and Leighton Coates[6,a)]

AFFILIATIONS

[1] Eppley Institute for Cancer and Allied Diseases, 986805 Nebraska Medical Center, Omaha, Nebraska 68198-6805, USA
[2] Biomolecular Measurement Division, National Institute of Standards and Technology, Gaithersburg, Maryland 20899, USA and Institute for Bioscience and Biotechnology Research, Rockville, Maryland 20850, USA
[3] Department of Biochemistry, Center for Structural Biology, Vanderbilt University, School of Medicine, Nashville, Tennessee 37232-0146, USA
[4] Molecular Biophysics and Integrated Bioimaging Division, Lawrence Berkeley National Laboratory, Berkeley, California 94720, USA
[5] Neutron Scattering Division, Oak Ridge National Laboratory, 1 Bethel Valley Road, Oak Ridge, Tennessee 37831, USA
[6] Second Target Station, Oak Ridge National Laboratory, 1 Bethel Valley Road, Oak Ridge, Tennessee 37831, USA
[7] Department of Biochemistry and the Redox Biology Center, University of Nebraska-Lincoln, Lincoln, Nebraska 68588, USA
[8] Department of Biochemistry and Molecular Biology, Indiana University School of Medicine, 635 Barnhill Drive, Indianapolis, Indiana 46202, USA
[9] Center for Advanced Mathematics in Energy Research Applications, Lawrence Berkeley National Laboratory, Berkeley, California 94720, USA

Note: Paper published as part of the Special Topic on New Science Opportunities at the Spallation Neutron Source Second Target Station.
[a)]**Author to whom correspondence should be addressed:** coatesl@ornl.gov

ABSTRACT

Revealing the positions of all the atoms in large macromolecules is powerful but only possible with neutron macromolecular crystallography (NMC). Neutrons provide a sensitive and gentle probe for the direct detection of protonation states at near-physiological temperatures and clean of artifacts caused by x rays or electrons. Currently, NMC use is restricted by the requirement for large crystal volumes even at state-of-the-art instruments such as the macromolecular neutron diffractometer at the Spallation Neutron Source. EWALD's design will break the crystal volume barrier and, thus, open the door for new types of experiments, the study of grand challenge systems, and the more routine use of NMC in biology. EWALD is a single crystal diffractometer capable of collecting data from macromolecular crystals on orders of magnitude smaller than what is currently feasible. The construction of EWALD at the Second Target Station will cause a revolution in NMC by enabling key discoveries in the biological, biomedical, and bioenergy sciences.

INTRODUCTION

Biological research and its resultant applications provide a wide range of benefits to society. The benefits are especially conspicuous in human health and medicine but also pervade society in areas such as agriculture, food, consumer products, biofuels, materials, environmental protection, national security, and industrial processes. This research is the key to new technologies and sustainable prosperity. Natural systems reflect a mastery of physical laws and engineering principles against which the best artificial systems look primitive. This mastery by nature spans catalysis, energy conversion, materials synthesis, sensing, communications, and computation,

among other areas. In addition to performing these functions, biological systems are self-organizing, self-assembling, adaptive, and robust while operating far from equilibrium. EWALD will enable such systems to be studied in unprecedented detail and allow scientists to achieve innovative experiments that are far beyond the limits of current instruments. By reverse-engineering biological machines in atomic detail, the first principles of engineering will be advanced for future applications to new products and processes.

Neutron crystallography offers many advantages. Neutron density maps provide exquisite, unbiased structural data about hydrogen positions. With these data, the binding sites of active site solvent, substrate, and product, the protonation state of ligands, and the source of the protons in a reaction can be precisely and exactly identified. Moreover, hydrogen positions around heavy metal centers, whose dominating electron density masks nearby protons in x-ray structures, can be unambiguously located with neutrons. Crucially, neutron beams do not reduce metal centers and do not cause radiation damage. Without radiation damage, cryocooling of the crystal is not a necessity, and room-temperature (RT), capillary-mounted crystals can be used for data collection. Unlike with x rays, cryo-neutron crystallography is used for the single purpose of trapping reaction intermediates (Azadmanesh *et al.*, 2021; 2022; Casadei *et al.*, 2014; Coates *et al.*, 2014; Kwon *et al.*, 2018; and Blakeley *et al.*, 2004). Furthermore, the combination of RT capillary mounts and the nonreducing neutron beam allows the continuous maintenance of the crystal redox state through vapor diffusion (Azadmanesh *et al.*, 2018). Such maintenance of the redox state is extremely important, for example, to track the detailed locations of never-before-seen hydrogen positions in metalloenzymes that employ concerted proton-electron transfers (CPETs), such as human mitochondrial manganese superoxide dismutase (Azadmanesh *et al.*, 2021) or human heme peroxidase (Casadei *et al.*, 2014; Kwon *et al.*, 2016). Here, candidate approaches are not necessary (e.g., point mutation or site-specific labeling), and the hydrogen atom positions of the entire enzyme are solved in an unbiased manner. The unique long wavelength and high brightness source characteristics of the STS mean that EWALD will fundamentally advance the field of neutron crystallography by promoting the rapid neutron diffraction data collection from small crystal samples that are relatively easy to grow. Some "grand challenge" examples are detailed below to show the exciting science that EWALD will make possible.

PHOTOSYNTHESIS—PROVIDING OXYGEN FOR LIFE ON EARTH

Most oxygen in the atmosphere is generated by plants, algae, and cyanobacteria through the photo-induced oxidation of water to oxygen gas (O_2). This reaction also lies at the heart of efforts to create artificial photosynthetic systems for converting solar energy to fuels. In photosynthetic organisms, the reaction is catalyzed by the multi-subunit membrane protein photosystem II (PS-II, Fig. 1). The oxygen-evolving complex (OEC) of PS-II contains a metal cluster (Mn_4CaO_5) that catalyzes the oxidation of H_2O to O_2 (Yano and Yachandra, 2014); that metal cluster is known to be reduced and damaged by x rays during the collection of the diffraction data (Yano *et al.*, 2005). EWALD will provide the experimental apparatus needed to study the neutron structure of PS-II without radiation

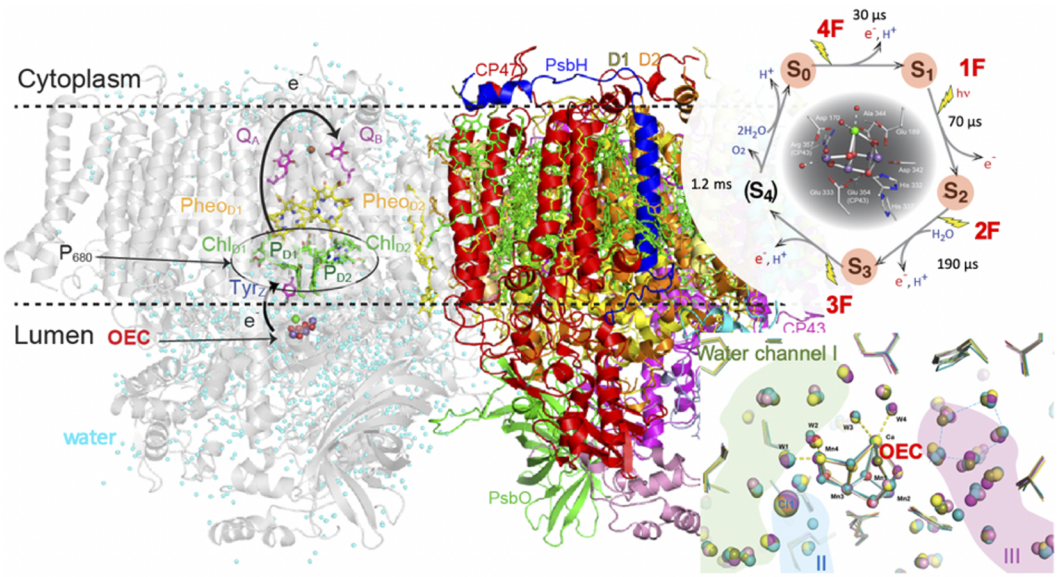

FIG. 1. The photosynthetic dimeric PS-II complex (left) is a multi-component, hierarchical assembly tuned to optimize the capture of available light and maximize the efficiency of energy conversion. The first step in photosynthesis is light capture by antennae complexes within the thylakoid membranes (dashed lines) that absorb and transfer solar energy to PS-II, where water-splitting at the OEC within PS-II occurs via the Kok cycle (right). The OEC is connected to the bulk water by several water channels (bottom right) and the water molecules in its vicinity change position in different illumination states, highlighting the importance of the details of the H-bond network for the catalytic cycle.

damage and reduction of the metal cluster. The all-atom structures provided will be fascinating as they reveal how photosynthesis provides oxygen for life on earth.

When H_2O is oxidized, it produces O_2 and protons and sequentially releases four electrons for each oxygen molecule produced. This light-induced reaction is thought to involve a five-state kinetic model for photosynthetic oxygen evolution, known as the Kok cycle. While x-ray structures have begun to unveil details of the mechanism of this reaction (Kern, 2018; Suga, 2019; and Ibrahim, 2020), the underlying chemistry is complex, and many key questions remain unanswered, including (1) the role of the individual metals in the cluster and their effect on the surrounding protein active site, (2) the role of hydrogen bonding waters, and (3) how the substrate (water) enters and the products (protons and oxygen) exit the active site. To obtain a detailed understanding of how PS-II works the new capabilities of the STS and EWALD will be vital.

The exact order in which manganese oxidation occurs in the photo-induced Kok cycle is not known and to accurately study the concerted proton-electron transfers requires a probe that does not reduce metal centers (Yano *et al.*, 2005). Neutrons are, thus, ideally suited to follow oxygen evolution, as PS-II crystals are moved among the four (meta)stable intermediates using laser pumping, enabling data to be collected in a pump–probe approach combined with cryotrapping. Recent progress has been made in the growth of larger crystals up to 0.5 mm^3 of PS-II for neutron diffraction studies by the Yano group (Hussein *et al.*, 2018). Large volume, neutron-diffraction quality crystals are difficult to grow, as PS-II crystals contain a large macromolecular complex consisting of several subunits, coupled with a high solvent content (70%). Thus, unfortunately, data collection has not been feasible on MaNDi. Smaller crystals generally diffract better due to fewer imperfections and ease of handling. Thus, EWALD would completely enable this exciting project that is waiting for this technological breakthrough.

EWALD will reveal many fascinating aspects of PS-II catalysis. Specifically, collecting data in the stable, dark, ground state (S1) at room temperature would reveal the protonation pattern for many residues in the environment of the Mn cluster involved in fine tuning of the hydrogen bonding network necessary for optimum efficiency of the catalyst. Beyond the dark state, it will be possible to collect data for different semistable states (Fig. 1, Figs. S2, S3, and S0) by flash freezing samples after illumination and collection under cryogenic conditions. Previous data indicate that different channels within the protein are used for proton transport during different steps in the reaction cycle. Detecting changes in the hydrogen bonding pattern for different S-states will give a better understanding of the regulation of the catalytic site along the reaction cycle and how proton-egress is spatially tuned during water oxidation in PS-II. Importantly, recent x-ray diffraction data indicate a change in the hydrogen bonding network in the water channels that connect the Mn cluster to the bulk solvent (Hussein *et al.*, 2021), and elucidating the precise nature of these changes via neutron diffraction at EWALD would allow a better understanding of the intricate regulation of proton and water transfer around the oxygen evolving complex (Hussein *et al.*, 2021).

EWALD also would elucidate the nature of the substrate water. Ammonia was shown to bind to the metal cluster by spectroscopic methods by replacing one of the non-substrate waters (Boussac *et al.*, 1990); hence, the replaced water can be excluded as a candidate for the substrate water. However, efforts to distinguish ammonia vs water by x-ray crystallography (Young *et al.*, 2016) are complicated by the nearly identical size of the resulting electron density for both molecules and the substrate water position cannot be defined. Neutron diffraction, in contrast, would allow ND_3 to be clearly identified due to its trigonal pyramidal shape in the resulting maps and could, hence, help to identify the location of the first substrate bound to the Mn-cluster, which, in turn, has direct implications for the possible mechanism of O_2 bond formation. In this way, the wealth of all-atom structures of PS-II obtained with EWALD empower the field of photosynthetic catalysis.

PANDEMIC PREPAREDNESS—DRUG DESIGN TO PROTECT FROM THE NEXT PANDEMIC

The coronavirus disease-19 (COVID-19) pandemic caught the world by surprise in early 2020 and unfortunately continues after two years of disrupting global travel, economic activities, and devastating the lives of many people on the planet (Hussain *et al.*, 2020). The etiological agent responsible for the deadly COVID-19 is a novel coronavirus SARS-CoV-2, a cousin of the Severe Acute Respiratory Syndrome (SARS-CoV) and the Middle East Respiratory Syndrome coronaviruses (MERS-CoV), with each causing separate pandemics in 2003 and 2012, respectively. Vaccines and small-molecule therapeutic intervention options have been developed in record time to stop the spread of SARS-CoV-2 (Callaway, 2020 and Owen *et al.*, 2021).

Emergence of SARS-CoV-2 has demonstrated that easily transmissible respiratory viruses can become the agents of future pandemics, as many people can be rapidly infected by the lingering aerosols containing viral particles generated through coughing, sneezing, and even simply talking. Different coronaviruses, and other single-stranded positive-sense RNA viruses such as rhinoviruses, noroviruses, and enteroviruses, share a lot of similarities in the proteins encoded in their genomes. Consequently, one of the strategies in the development of small-molecule therapeutics is the design of broad-spectrum antiviral drugs, for instance, pan-coronavirus inhibitors of viral proteins (Liu *et al.*, 2020; Gil *et al.*, 2020). Some of the proteins encoded in coronavirus genomes, including main protease (M^{pro}), papain-like protease (PL^{pro}), and RNA-dependent RNA polymerase (RdRp), are known drug targets. Knowledge of how these enzymes function and interact with small-molecule inhibitors at the atomic level, including accurate determination of protonation states, their changes, and hydrogen bonding networks, is of great importance to guide structure-based and computer-assisted drug design. This information can only be obtained with NMC.

The neutron crystal structures of ligand-free and of covalent and noncovalent inhibitor-bound SARS-CoV-2 M^{pro} have been determined (Fig. 2) allowing the direct observation of the protonation states of all residues in a coronavirus protein for the first time (Kneller *et al.*, 2020; 2021a; and 2021b). At rest, the catalytic Cys–His dyad exists in the reactive zwitterionic state, with both Cys145 and His41 charged, instead of the anticipated neutral state. Covalent inhibitor binding results in modulation of the protonation states (Kneller *et al.*, 2021), retaining the overall electric charge of the M^{pro} active site cavity—a result that was not predicted by computer simulations (Pavlova *et al.*, 2021). Many more neutron structures of

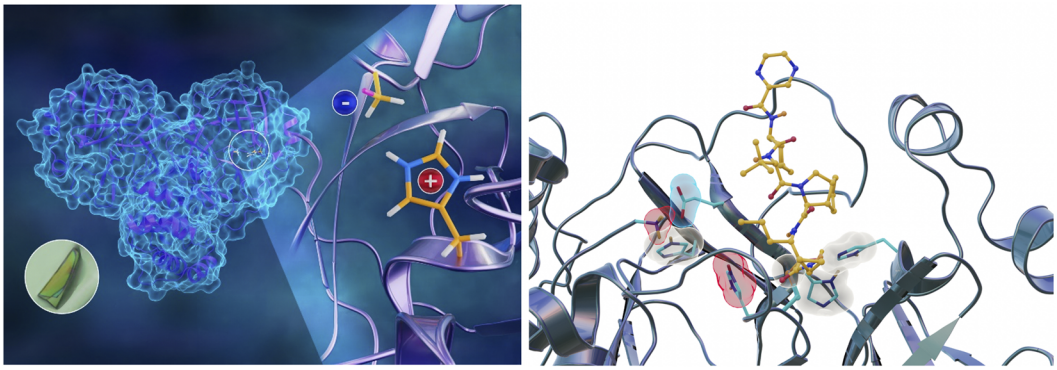

FIG. 2. SARS-CoV-2 main protease enzyme plays an indispensable role in the virus's replication process, and the enzyme is a target for the design of small-molecule drugs. (left) Neutron diffraction experiments revealed unexpected electrical charges in the amino acids cysteine (negative) and histidine (positive) where the chemical reaction occurs, underpinning the virus's replication. The inset features a crystal sample of the protease, grown and studied at near physiological temperature, resulting in the first neutron structure of the enzyme. (right) Protonation states of ionizable amino acid residues (red positive protonated His, gray neutral His, blue negative Glu) were observed with neutron crystallography upon a covalent inhibitor binding (yellow), providing essential information for the design of specific SARS-CoV-2 main protease inhibitors. Targeting the enzyme with specific protease inhibitors designed to efficiently bind to the newly discovered electrical charged states can effectively stop the "heart" of the virus, killing it before it has a chance to reproduce.

M^{pro} are needed, with various covalent and non-covalent inhibitors and with substrates or substrate analogs, to obtain a full picture of the enzyme function and inhibition. PL^{pro} and RdRp are more challenging targets for NMC because they do not produce large crystals and the unit cell parameters can be >200 Å. To protect from future pandemics, EWALD can make these studies realized.

EWALD OPTICS DESIGN AND PERFORMANCE

The science case articulated for EWALD identifies the need for a single crystal diffractometer optimized for the study of small crystal volumes below 0.01 mm^3 with unit cell edges between 10 and 300 Å. We expect measurements on such crystal volumes to take place between 5 and 7 days depending on the space group of the crystal being collected. EWALD has been designed to transport neutrons with wavelengths between 1.5 and 4.5 Å with a maximum beam size of 1 mm^2 at the sample position, which provides the flexibility to study larger crystals when they are available. The neutron optics system for EWALD is based on a pair of nested Kirkpatrick Baez (KB) focusing neutron supermirrors located at 25.7 and 80.6 m from the moderator, respectively. These neutron supermirrors are 5.0 and 7.0 m in length and 17 and 14 cm in height, respectively. They image the moderator at the second source located at 45.3 m from the moderator and then to the sample position. A neutron absorbing slit is placed at the secondary source to alter the beam size at the sample position (Fig. 3).

The opening of the slit at the secondary source will be demagnified (focused) by a factor of ~100× (in area) at the sample position. By varying the size of the slit opening, we will be able to adjust the dimensions of the neutron beam at the sample position down to 0.01 mm^2. Using this mechanism, we will closely match the beam size at the sample position to the dimensions of the crystal

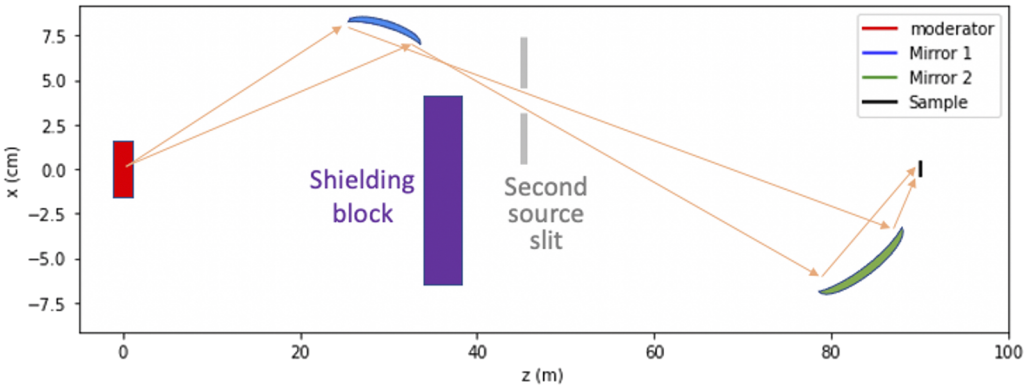

FIG. 3. An illustration of the EWALD optical design. It consists of a pair of nested Kirkpatrick Baez mirrors (Montel optics). Only dimensions along x (horizontal and perpendicular to the beam) are shown since the vertical direction is symmetrical at the cross section and the dimensions are identical. In this concept, the direct line of sight to the moderator is blocked by shielding.

to reduce background and increase the signal-to-noise ratio. Using this arrangement, we also have no line of sight from the moderator to the sample position, further reducing the background while preventing any fast neutrons and gammas produced during neutron production from reaching the sample position. The horizontal and vertical divergence of the neutron beam at the sample is fixed by the KB mirror system at up to 0.42° FWHM across the wavelength band. The brilliance transfer of the EWALD neutron optics is 73% across the 1.5–4.5 Å wavelength band, as shown in Fig. 4, showing that the EWALD optics are highly efficient at transporting cold neutrons to the sample position.

MaNDi at the Spallation Neutron Source is located on a decoupled hydrogen moderator that gives sharp neutron pulses with short emission times (17.4 μs FWHM at 2 Å), enabling the study of large unit cell axes up to 300 Å. The moderator pulse width at STS for the cylindrical 3 × 3 cm^2 high-brightness coupled moderator is 43.3 μs FWHM at 2 Å. Therefore, to ensure the same or better wavelength resolution for EWALD at the STS, an instrument length of three times longer is required to account for the moderator pulse width difference. Thus, EWALD has an incident flight path length of 90 m, three times that of MaNDi. At 90 m and with a 15 Hz repetition rate of the STS, EWALD will have a bandwidth ($\Delta\lambda$) of 3.0 Å, perfect for NMC as all useful wavelengths (1.5–4.5 Å) can be collected in a single exposure. Using the *McVine* program (Lin *et.al.*, 2016; 2019), we have conducted several initial Monte Carlo simulations of EWALD to assess its performance relative to that of MaNDi at the first target station of SNS. On MaNDi (Coates *et al.*, 2010; 2015; 2017; and 2018) with a fixed beam divergence of 0.38° at the sample position, the flux on the sample is 1.3 × 10^5 n mm^{-2} s^{-1} for all neutrons between 2 and 4.16 Å. The higher-brightness coupled moderator available at the STS combined with a KB neutron optics system has enabled us to increase the flux on the sample at EWALD to 2.83 × 10^6 n mm^{-2} s^{-1} for all neutrons between 1.5 and 4.5 Å, with a similar fixed beam divergence of 0.42°, giving us a 20-fold simulated gain factor in flux.

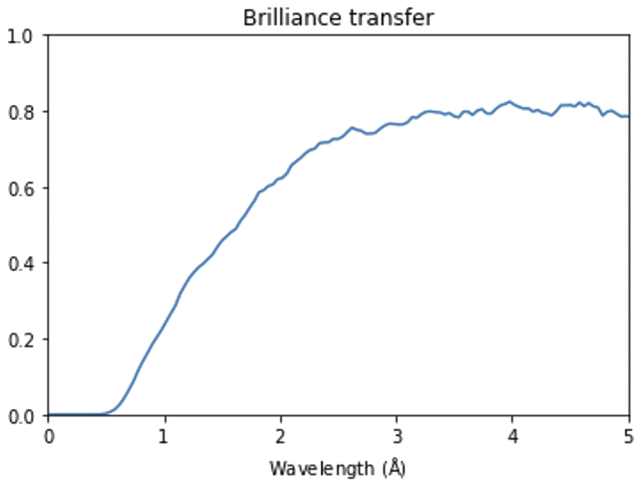

FIG. 4. Brilliance transfer vs wavelength in Ångstrom for the EWALD neutron optics design.

A list of the key instrument components of the EWALD instrument is given in Table I.

EWALD ENDSTATION

The end station of the Ewald instrument uses 37 High Resolution SNS Anger cameras, which are mounted on a hemispherical movable detector array frame that surrounds the sample (Fig. 5). The detector array can easily be retracted to allow access to the sample position for robotic sample changes.

The sample is surrounded by 37 silicon photomultiplier-based Anger cameras with a sample to detector distance of 0.34 m. This provides a solid angle coverage of 5.3 steradians enabling Bragg reflections to be measured up to 2-theta angles of 160°; thus, data can be recorded up to a maximum resolution of d_{min} = 0.6 Å. The high-solid-angle detector coverage coupled with the wide wavelength band enabled at STS enables the simultaneous measurement of large volumes of reciprocal space, minimizing the number of crystal rotations required to collect a complete dataset. These key characteristics will allow EWALD to collect high-resolution single-crystal diffraction data on small and large molecules using crystal volumes as low as 0.1 to 0.001 mm^3 with a minimal number of orientations.

NEW SCIENTIFIC OPPORTUNITIES ON EWALD

STS offers unprecedented peak brightness and a broader energy range for each incident neutron pulse and much greater overall flux at the longer wavelengths that are essential for biological studies. Furthermore, innovations in neutron optics and other technologies, such as dynamic nuclear polarization (DNP), will provide instrument performance gains of two orders of magnitude or more. DNP enables spin polarization of the hydrogen atoms in the sample, which drastically changes the coherent and incoherent neutron scattering cross-sections of hydrogen in ideal cases amplifying the coherent scattering by almost an order of magnitude and suppressing the incoherent background to zero (Sturhamm, 2004; Piegsa *et al.*, 2013; Pierce *et al.*, 2019; and 2020).

Together, these improvements will dramatically reduce data collection times while also allowing the use of smaller samples, an important consideration because most biological samples are difficult to obtain in sufficient volumes. Smaller samples and beam sizes will allow the characterization of new biological systems (Fig. 6), expanding by several-fold the number and classes of biological problems that can be investigated. It is expected that net gains for NMC will be transformative, allowing precision analysis of much larger molecular complexes than currently possible and with far smaller crystals.

EWALD FUTURE OUTLOOK

The EWALD instrument at STS possesses the ability to resolve neutron wavelengths enabling data collection on large unit cells with the higher neutron flux on the sample that is typically seen at a reactor. This combination of high wavelength resolution and increased neutron flux means that EWALD will be a unique instrument in the global landscape. Reactor-based quasi-Laue instrumentation such as IMAGINE at HFIR (Meilleur *et al.*, 2013) and LADI at ILL (Blakeley *et al.*, 2010) excel in studying protein crystals with unit

TABLE I. Primary EWALD instrument components.

Component	Description	Location from the moderator
	Beam delivery	
Flight tube	Evacuated flight tube	0.9 − 89.8 m
Slit	Defines beam size at the sample position	Z = 45.3 m
First bandwidth chopper	1 disk at 15 Hz, defines bandwidth	Z = 8.5 m
Second bandwidth chopper	1 disk at 15 Hz, defines bandwidth	Z = 10.5 m
First mirror	Steerable KB mirror	Z = 25.7 m
Operations shutter	Primary shutter for daily operations	Z = 81.3 m
Second mirror	Steerable KB mirror	Z = 80.6 m
Flight tube	Evacuated flight tube	Z = 5.9 − 89.9 m
Beamline shielding	Bunker to cave	Z = 13.2 − 86.4 m
Sample location	Sample	Z = 90 m
Component	Description	Location from Sample
	End station	
Shield cave		Z = −3.6 ± 3.0 m
Detector array	37 silicon photo-multiplier detectors providing 5.3 sr coverage	R = 0.34 m
Goniometer	Sample positioning for crystals	Z = 0 m

cell dimensions less than 100 Å but struggle with spatial reflection overlap on larger unit cells. Monochromatic reactor-based instrumentation such as BIODIFF (Ostermann and Schrader, 2015) at FRM-II trade neutron bandwidth for flux to decrease reflection density lowering spatial overlap to increase the size of unit cells that can be studied at reactor-based sources up to 180 Å. The iBIX beamline at the J-PARC spallation source (Taneka *et al.*, 2009) can collect data on unit cells up to 135 Å, while the NMX beamline at the European Spallation Source is currently under construction in Sweden and is currently due to complete in 2027 and start operations at 2 MW. The long pulse length of the ESS provides a high flux of neutrons at the sample position but with low time resolution meaning that NMX can collect data on unit cells up to 180 Å before reflections spatially overlap. MaNDi at the SNS (Coates *et al.*, 2015) can resolve unit cell dimensions up to 300 Å but with 20 times lower flux meaning that EWALD will be able to collect data from systems that are not currently feasible on MaNDi. The EWALD instrument concept occupies a unique space in neutron diffraction instrumentation worldwide, offering the ability to collect on unit cell edges up to 300 Å with a neutron flux higher than that of a reactor-based instrument such as LADI (Table II). DALI at the Institut Laue-Langevin (ILL) is a new instrument currently under commissioning that is expected to have superior performance to LADI.

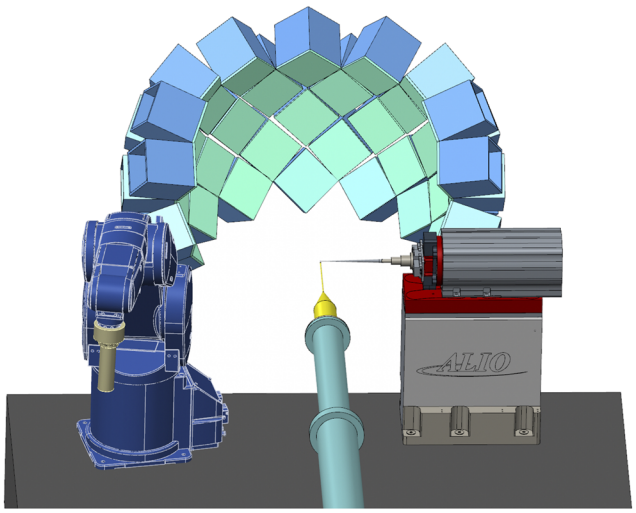

FIG. 5. An engineering model of the Ewald end station is shown. A large detector array composed of 37 High Resolution SNS Anger cameras is designed to reduce the number of orientations required to collect a complete dataset. A high-resolution goniometer, nitrogen cryostream, and robotic sample changer will allow for offsite operation.

SOFTWARE FOR DATA REDUCTION

The Daresbury software suite has reduced neutron Laue data for many years (Helliwell *et al.*, 1989; Campbell *et al.*, 1998). It is well suited to reducing neutron data collected at reactor-based instruments. At a spallation neutron source such as the STS, SNS, J-PARC, or ESS, a different approach to data reduction is required to enable the benefits of time-of-flight data. These include reduced experimental background and the ability to collect on large unit cells. Recently, new algorithms have been developed and deployed to utilize 3D profile fitting of neutron time-of-flight diffraction data (Sullivan *et al.*, 2018). This new method has produced significantly more accurate data than previously used methods enabling new scientific discoveries. EWALD and the next generation of spallation neutron protein crystallography instruments will utilize 3D

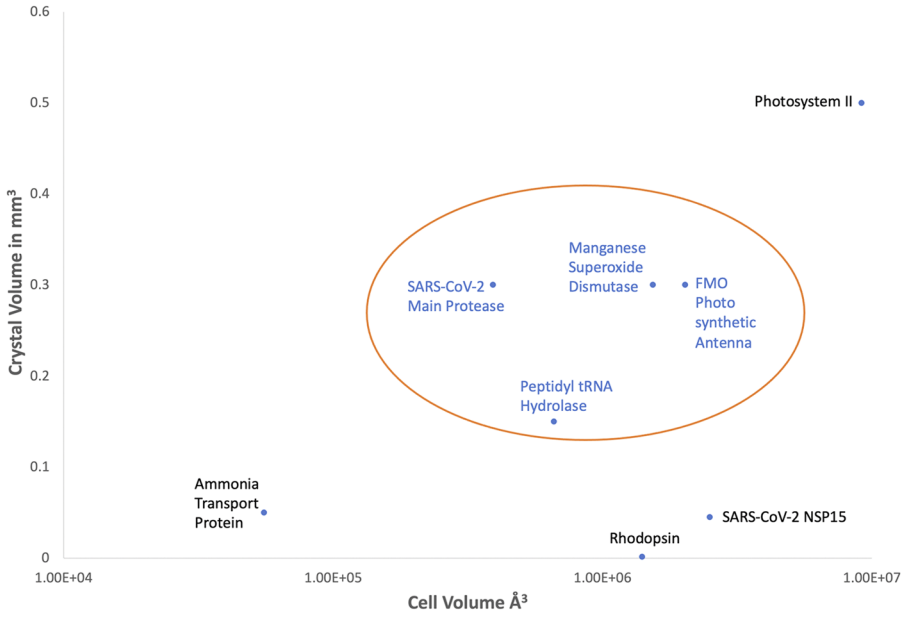

FIG. 6. A scatter plot of examples of challenging protein crystals collected on MaNDi (blue text) and several examples of protein crystals that the Ewald instrument can bring into range for neutron crystallography (black text). The orange ellipse shows an empirical limit that has been observed on the MaNDi instrument.

TABLE II. Comparison of current and future NMX instruments.

Instrument	Flux at sample (n cm^{-2} s^{-1})	Max unit cell (Å)
BIODIFF	8.0×10^6	180
DALI	$>1.1 \times 10^8$	150
EWALD	2.8×10^8	300
LADI	1.1×10^8	150
iBIX	7.0×10^7	135
IMAGINE	3.0×10^7	150
MaNDi	1.3×10^7	300
NMX (2 MW)[a]	4.0×10^8	180
NMX (5 MW)[a]	1.0×10^9	180

[a]Estimates based upon a brilliance transfer of 50%.

profile fitting to integrate Bragg reflections from smaller and smaller crystals.

CONCLUSIONS

The current generation of macromolecular neutron instrumentation can collect data on crystals below a millimeter in volume, representing an order of magnitude improvement over the previous generation of neutron instrumentation. Currently, a minimum crystal volume of ~0.3 mm^3 (0.7 × 0.7 × 0.6 mm^3) is required for neutron studies. The EWALD instrument at the STS offers the ability to collect data on crystal volumes below 0.01 mm^3 (0.3 × 0.3 × 0.1 mm^3) while being capable of resolving unit cells up to 300 Å on edge. This reduced sample size requirement will enable new biological systems and smaller crystals to be studied with neutrons that are beyond the reach of current instrumentation. The EWALD instrument is currently in the concept phase and is not expected to become available until after 2032.

ACKNOWLEDGMENTS

This research used resources at the SNS and the HFIR, which are DOE Office of Science User Facilities operated by the Oak Ridge National Laboratory (ORNL). This research used resources of the Spallation Neutron Source Second Target Station Project at ORNL under Grant No. ERKC2TS. ORNL is managed by UT-Battelle LLC for DOE's Office of Science, the single largest supporter of basic research in the physical sciences in the United States.

AUTHOR DECLARATIONS

Conflict of Interest

The authors have no conflicts to disclose.

DATA AVAILABILITY

The data that support the findings of this study are available from the corresponding author upon reasonable request.

REFERENCES

Azadmanesh, J., Lutz, W. E., Coates, L., Weiss, K. L., and Borgstahl, G. E. O., "Direct detection of coupled proton and electron transfers in human manganese superoxide dismutase," Nat. Commun. **12**, 2079 (2021).

Azadmanesh, J., Lutz, W. E., Coates, L., Weiss, K. L., and Borgstahl, G. E. O., "Cryotrapping peroxide in the active site of human mitochondrial manganese superoxide dismutase crystals for neutron diffraction," Acta Crystallogr., Sect. F **78**, 8–16 (2022).

Azadmanesh, J., Lutz, W. E., Weiss, K. L., Coates, L., and Borgstahl, G. E. O., "Redox manipulation of the manganese metal in human manganese superoxide dismutase for neutron diffraction," Acta Crystallogr., Sect. F **74**, 677–687 (2018).

Blakeley, M. P., Kalb, A. J., Helliwell, J. R., and Myles, D. A. A., "The 15-K neutron structure of saccharide-free concanavalin A," Proc. Natl. Acad. Sci. U. S. A. **101**(47), 16405–16410 (2004).

Blakeley, M. P., Teixeira, S. C., Petit-Haertlein, I., Hazemann, I., Mitschler, A., Haertlein, M., Howard, E., and Podjarny, A. D., "Neutron macromolecular crystallography with LADI-III," Acta Crystallogr., Sect. D **66**(Pt 11), 1198 (2010).

Boussac, A., Rutherford, A. W., and Styring, S., "Interaction of ammonia with the water splitting enzyme of photosystem II," Biochemistry **29**(1), 24–32 (1990).

Callaway, E., "COVID vaccine excitement builds as Moderna reports third positive result," Nature **587**, 337–338 (2020).

Campbell, J. W., Hao, Q., Harding, M. M., Nguti, N. D., and Wilkinson, C., J. Appl. Crystallogr. **31**, 496–502 (1998).

Casadei, C. M., Gumiero, A., Metcalfe, C. L., Murphy, E. J., Basran, J., Concilio, M. G., Teixeira, S. C. M., Schrader, T. E., Fielding, A. J., Ostermann, A., Blakeley, M. P., Raven, E. L., and Moody, P. C. E., "Heme enzymes. Neutron cryo-crystallography captures the protonation state of ferryl heme in a peroxidase," Science **345**(6193), 193–197 (2014).

Coates, L., Cao, H. B., Chakoumakos, B. C. *et al.*, "A suite-level review of the neutron single-crystal diffraction instruments at Oak Ridge National Laboratory," Rev. Sci. Instrum. **89**(9), 092802 (2018).

Coates, L., Cuneo, M. J., Frost, M. J. *et al.*, "The macromolecular neutron diffractometer MaNDi at the Spallation Neutron Source," J. Appl. Crystallogr. **48**, 1302–1306 (2015).

Coates, L. and Robertson, L., "Ewald: An extended wide-angle Laue diffractometer for the second target station of the Spallation Neutron Source," J. Appl. Crystallogr. **50**, 1174–1178 (2017).

Coates, L., Stoica, A. D., Hoffmann, C., Richards, J., and Cooper, R., "The macromolecular neutron diffractometer (MaNDi) at the Spallation Neutron Source, Oak Ridge: Enhanced optics design, high-resolution neutron detectors and simulated diffraction," J. Appl. Crystallogr. **43**(3), 570–577 (2010).

Coates, L., Tomanicek, S., Schrader, T. E., Weiss, K. L., Ng, J. D., Jüttner, P., and Ostermann, A., "Cryogenic neutron protein crystallography: Routine methods and potential benefits," J. Appl. Crystallogr. **47**(4), 1431–1434 (2014).

Gil, C., Ginex, T., Maestro, I., Nozal, V., Barrado-Gil, L., Cuesta-Geijo, M. Á., Urquiza, J., Ramírez, D., Alonso, C., Campillo, N. E., and Martinez, A., "COVID-19: Drug targets and potential treatments," J. Med. Chem. **63**, 12359–12386 (2020).

Helliwell, J. R., Habash, J., Cruickshank, D. W. J., Harding, M. M., Greenhough, T. J., Campbell, J. W., Clifton, I. J., Elder, M., Machin, P. A., Papiz, M. Z., and Zurek, S., "The recording and analysis of Laue diffraction photographs," J. Appl. Crystallogr. **22**, 483–497 (1989).

Hussain, A., Yadav, S., Hadda, V., Suri, T. M., Tiwari, P., Mittal, S., Madan, K., and Mohan, A., "Covid-19: A comprehensive review of a formidable foe and the road ahead," Expert Rev. Respir. Med. **14**, 869–879 (2020).

Hussein, R., Ibrahim, M., Bhowmick, A. *et al.*, "Structural dynamics in the water and proton channels of photosystem II during the S_2 to S_3 transition," Nat. Commun. **12**, 6531 (2021).

Hussein, R., Ibrahim, M., Chatterjee, R. *et al.*, "Optimizing crystal size of photosystem II by macroseeding: Toward neutron protein crystallography," Cryst. Growth Des. **18**(1), 85–94 (2018).

Ibrahim, M. *et al.*, "Untangling the sequence of events during the $S_2 \rightarrow S_3$ transition in photosystem II and implications for the water oxidation mechanism," Proc. Natl. Acad. Sci. U. S. A. **117**, 12624–12635 (2020).

Kern, J. *et al.*, "Structures of the intermediates of Kok's photosynthetic water oxidation clock," Nature **563**, 421–425 (2018).

Kneller, D. W., Li, H., Galanie, S., Phillips, G., Labbé, A., Weiss, K. L., Zhang, Q., Arnould, M. A., Clyde, A., Ma, H., Ramanathan, A., Jonsson, C. B., Head, M. S., Coates, L., Louis, J. M., Bonnesen, P. V., and Kovalevsky, A., "Structural, electronic, and electrostatic determinants for inhibitor binding to subsites S1 and S2 in SARS-CoV-2 main protease," J. Med. Chem. **64**(23), 17366–17383 (2021).

Kneller, D. W., Phillips, G., Weiss, K. L., Pant, S., Zhang, Q., O'Neill, H. M., Coates, L., and Kovalevsky, A., "Unusual zwitterionic catalytic site of SARS-CoV-2 main protease revealed by neutron crystallography," J. Biol. Chem. **295**, 17365–17373 (2020).

Kneller, D. W., Phillips, G., Weiss, K. L., Zhang, Q., Coates, L., and Kovalevsky, A., "Direct observation of protonation states modulation in SARS-CoV-2 main protease upon inhibitor binding with neutron crystallography," J. Med. Chem. **64**(8), 4991–5000 (2021a).

Kneller, D. W., Zhang, Q., Coates, L., Louis, J. M., and Kovalevsky, A., "Michaelis-like complex of SARS-CoV-2 main protease visualized by room temperature X-ray crystallography," IUCrJ **8**, 973–979 (2021b).

Kwon, H., Basran, J., Casadei, C. M. *et al.*, "Direct visualization of a Fe(IV)–OH intermediate in a heme enzyme," Nat. Commun. **7**, 13445 (2016).

Kwon, H., Langan, P. S., Coates, L., Raven, E. L., and Moody, P. C. E., "The rise of neutron cryo-crystallography," Acta Crystallogr., Sect. D **74**, 792–799 (2018).

Lin, J. Y. Y., Islam, F., Sala, G., Lumsden, I., Smith, H., Doucet, M., Stone, M. B., Abernathy, D. L., Ehlers, G., Ankner, J. F., and Granroth. G. E., "Recent developments of MCViNE and its applications at SNS," J. Phys. Commun. **3**, 085005 (2019).

Lin, J. Y. Y., Smith, H. L., Granroth, G. E., Abernathy, D. L., Lumsden, M. D., Winn, B., Aczel, A. A., Aivazis, M., and Fultz. B., "MCViNE - An object oriented Monte Carlo neutron ray tracing simulation package," Nucl. Instrum. Methods Phys. Res., Sect. A **810**, 86–99 (2016).

Liu, C., Zhou, Q., Li, Y., Garner, L. V., Watkins, S. P., Carter, L. J., Smoot, J., Gregg, A. C., Daniels, A. D., Jervey, S., and Albaiu, D., "Research and development on therapeutic agents and vaccines for COVID-19 and related human coronavirus diseases," ACS Cent. Sci. **6**, 315–331 (2020).

Meilleur, F., Munshi, P., Robertson, L., Stoica, A. D., Crow, L., Kovalevsky, A., Koritsanszky, T., Chakoumakos, B. C., Blessing, R., and Myles, D. A. A., Acta Crystallogr., Sect. D **69**, 2157–2160 (2013).

Ostermann, A. and Schrader, T., "BIODIFF: Diffractometer for large unit cells," J. Large-Scale Res. Facil. **1**, A2 (2015).

Owen, D. R., Allerton, C. M. N., Anderson, A. S., Aschenbrenner, L., Avery, M., Berritt, S., Boras, B., Cardin, R. D., Carlo, A., Coffman, K. J., Dantonio, A., Di, L., Eng, H., Ferre, R., Gajiwala, K. S., Gibson, S. A., Greasley, S. E., Hurst, B. L., Kadar, E. P., Kalgutkar, A. S., Lee, J. C., Lee, J., Liu, W., Mason, S. W., Noell, S., Novak, J. J., Obach, R. S., Ogilvie, K., Patel, N. C., Pettersson, M., Rai, D. K., Reese, M. R., Sammons, M. F., Sathish, J. G., Singh, R. S. P., Steppan, C. M., Stewart, A. E., Tuttle, J. B., Updyke, L., Verhoest, P. R., Wei, L., Yang, Q., and Zhu, Y., "An oral SARS-CoV-2 M^{pro} inhibitor clinical candidate for the treatment of COVID-19," Science **374**(6575), 1586–1593 (2021).

Pavlova, A., Lynch, D. L., Daidone, I., Zanetti-Polzi, L., Smith, M. D., Chipot, C., Kneller, D. W., Kovalevsky, A., Coates, L., Golosov, A. A., Dickson, C. J., Velez-Vega, C., Duca, J. S., Vermaas, J. V., Pang, Y. T., Acharya, A., Parks, J. M., Smith, J. C., and Gumbart, J. C., "Inhibitor binding influences the protonation states of histidines in SARS-CoV-2 main protease," Chem. Sci. **12**, 1513–1527 (2021).

Piegsa, F. M., Karlsson, M., van den Brandt, B., Carlile, C. J., Forgan, E. M., Hautle, P., Konter, J. A., McIntyre, G. J., and Zimmer, O., J. Appl. Crystallogr. **46**, 30–34 (2013).

Pierce, J., Crow, L., Cuneo, M., Edwards, M., Herwig, K. W., Jennings, A., Jones, A., Li, L., Meilleur, F., Myles, D. A. A., Robertson, L., Standaert, R., Wonder, A., and Zhao, J. K., Nucl. Instrum. Methods Phys. Res., Sect. B **940**, 430–434 (2019).

Pierce, J., Cuneo, M. J., Jennings, A., Li, L., Meilleur, F., Zhao, J., and Myles, D. A. A., "Dynamic nuclear polarization enhanced neutron crystallography: Amplifying hydrogen in biological crystals," Methods Enzymol. **634**, 153–175 (2020).

Stuhrmann, H. B., Rep. Prog. Phys. **67**, 1073 (2004).

Suga, M. *et al.*, "An oxyl/oxo mechanism for oxygen-oxygen coupling in PSII revealed by an x-ray free-electron laser," Science **366**, 334–338 (2019).

Sullivan, B., Archibald, R., Langan, P. S., Dobbek, H., Bommer, M., McFeeters, R. L., Coates, L., Wang, X., Gallmeier, F., Carpenter, J. M., Lynch, V., and Langan, P., "Improving the accuracy and resolution of neutron crystallographic data by three-dimensional profile fitting of Bragg peaks in reciprocal space," Acta Crystallogr., Sect. D **74**(11), 1085–1095 (2018).

Tanaka, I., Kusaka, K., Tomoyori, K., Niimura, N., Ohhara, T., Kurihara, K., Hosoya, T., and Ozeki, T., "Overview of a new biological neutron diffractometer (iBIX) in J-PARC," Nucl. Instrum. Methods Phys. Res., Sect. A **600**, 161–163 (2009).

Yano, J., Kern, J., Irrgang, K.-D. *et al.*, "X-ray damage to the Mn_4Ca complex in single crystals of photosystem II: A case study for metalloprotein crystallography," Proc. Natl. Acad. Sci. U. S. A. **102**(34), 12047–12052 (2005).

Yano, J. and Yachandra, V., "Mn_4Ca cluster in photosynthesis: Where and how water is oxidized to dioxygen," Chem. Rev. **114**, 4175–4205 (2014).

Young, I. D., Ibrahim, M., Chatterjee, R. *et al.*, "Structure of photosystem II and substrate binding at room temperature," Nature **540**(7633), 453–457 (2016).